



GEORG-AUGUST-UNIVERSITÄT
GÖTTINGEN



Bachelor's Thesis

A scaling law for magnetic fields of rapidly rotating stars

Ein Skalierungsgesetz für Magnetfelder schnell rotierender Sterne

prepared by

Merten Nikolay Dahlkemper

from Itzehoe

at the Institut für Astrophysik

Thesis period: 13. April 2016 until 20. Juli 2016

Supervisor: Dr. Denis Shulyak

First Referee: Prof. Dr. Ansgar Reiners

Second Referee: Dr. Frederick V. Hessmann

Abstract

Stellar magnetic fields and the processes which lead to their production are subject of current research. The aim of this thesis is to test a scaling law which describes the magnetic field strength of stars with convective zones. This scaling law is only applicable to stars which are fast rotating, i.e. their field is saturated and therefore not dependent on rotation rate. The analysis is done with *Modules for Experiments in Stellar Astrophysics* (MESA), which provides a powerful one-dimensional stellar evolution code. The result of this thesis is that dynamos of high mass stars ($M \gtrsim 1.0 M_{\odot}$) can produce magnetic fields with energy densities which are weaker than fields in low mass stars ($M \lesssim 0.6 M_{\odot}$) by a factor of three to four.

Keywords: stellar physics, magnetic fields, geodynamos, scaling law, MESA

Zusammenfassung

Magnetfelder von Sternen und die Prozesse, welche zu ihrer Erzeugung führen, sind Themen aktueller Forschung. Das Ziel dieser Arbeit ist es, ein Skalierungsgesetz zu testen, das die Magnetfeldstärke von Sternen mit konvektiven Zonen beschreibt. Dieses Skalierungsgesetz ist nur anwendbar auf Sterne, welche schnell rotieren, d.h. ein gesättigtes und damit von der Rotationsperiode unabhängiges Magnetfeld besitzen. Die Analyse wird mit MESA durchgeführt, einer Code-Bibliothek, welche einen mächtigen Sternentwicklungs-Code bereitstellt. Das Ergebnis dieser Arbeit ist, dass massive Sterne ($M \gtrsim 1.0 M_{\odot}$) magnetische Felder mit Energiedichten produzieren können, welche um einen Faktor drei bis vier schwächer sind als Felder von eher leichten Sternen ($M \lesssim 0.6 M_{\odot}$) liegen.

Stichwörter: stellare Physik, Magnetfelder, Geodynamos, Skalierungsgesetz, MESA

Contents

1	Introduction	1
2	Theoretical Foundations	3
2.1	Stellar Dynamos	3
2.1.1	Convective zones of stars	3
2.1.2	α - and Ω -effect	4
2.1.3	Saturated fields	5
2.2	Fundamental equations of Magnetohydrodynamics	5
2.2.1	Basic set of equations	6
2.2.2	Nondimensional numbers	7
2.3	Scaling laws for the magnetic fields of planets and stars	9
2.3.1	Elsasser number rule	9
2.3.2	Energy flux scaling	9
2.3.3	Application of energy flux scaling to stars	11
3	Numerical approach	13
3.1	Mixing-length theory of convection	13
3.2	MESA – Modules for Experiments in Stellar Astrophysics	14
3.3	Calculation of quantities	15
3.4	Choice of parameters	17
4	Results	19
4.1	Provided quantities	19
4.1.1	Radial Profiles	19
4.1.2	Overall values	20
4.2	Spatial distribution of efficiency factor	21
4.3	Magnetic Energy Densities	22
4.4	Comparison with Observations	24
4.4.1	Measuring stellar magnetic fields	24

Contents

4.4.2 Comparison	24
5 Discussion	37
5.1 Meaning of the results	37
5.2 Open questions	38
6 Conclusion	39
Bibliography	41

Nomenclature

Bold Letters, such as **E** refer to the corresponding vector quantities.

Latin Letters

variable	meaning	unit
E	Electrical field strength	$V/m = m \text{ kg}/s^3 A$
B	Magnetic flux density	$T = \text{kg}/s^2 A$
J	Electrical current density	A/m^2
u	Velocity	m/s
g	Gravitational acceleration	m/s^2
H	Scale height	m
q	Energy flux	$W/m^2 = \text{kg}/s^3$
c_p	Specific heat capacity at constant pressure	$J/K\text{kg} = m^2/K \text{ s}^2$
l	Length scale	m
E_{mag}	Magnetic energy density	J/m^3
F	Efficiency factor of field production	1
F_r	Radial dependent efficiency factor	1
r	Radius	m
R	Fixed radius of a planet or star	m
V	Volume	m^3
M	Mass	kg

Greek Letters

variable	meaning	unit
α	Thermal expansivity coefficient	$1/K$

Nomenclature

variable	meaning	unit
μ_0	Magnetic permeability of vacuum	$4\pi \times 10^{-7} \text{ N/A}^2 [= \text{kgm/s}^2\text{A}^2]$
ϵ_0	Permittivity of vacuum	$8.854 \times 10^{-12} \text{ C}^2/\text{Nm}^2 [= \text{A}^2\text{s}^4/\text{kgm}^3]$
ρ_e	Electrical charge density	$\text{C}/\text{m}^3 = \text{As}/\text{m}^3$
ρ	Mass density	kg/m^3
σ	Electrical conductivity	$1/\Omega\text{m} = \text{A}^2\text{s}/\text{m}^3\text{kg}$
τ	Time scale	s
η	Magnetic diffusivity	m^2/s
ν	Kinematic viscosity	m^2/s
κ	Thermal diffusivity	m^2/s
Ω	Rotation frequency	$1/\text{s}$
α_{MLT}	Mixing-length parameter	1

Indices

index	meaning
c	Convective
T	Temperature
p	Pressure
mag	Magnetic
\odot	Sun
0	At the surface

Abbreviations

abbreviation	meaning
LHS	Left Hand Side
MESA	Modules for Experiments in Stellar Astrophysics
MHD	Magnetohydrodynamics
RHS	Right Hand Side
r.m.s.	Root mean squared
EOS	Equation of state
yrs	Years

List of Figures

2.1	Schematic representation of convective zones in stars	4
2.2	Visualisation of Ω - and α -effect	4
2.3	Scaling law (2.25) applied to Earth, Jupiter and stars	12
4.1	Calibration of spectral types	23
4.2	Temperature profiles	26
4.3	Convective energy fluxes	27
4.4	Density profiles	28
4.5	Energy flux at the outer boundary	29
4.6	Average density	30
4.7a	Spatial distribution of F_r for $0.1 M_\odot \leq M \leq 0.3 M_\odot$	31
4.7b	Spatial distribution of F_r for $0.35 M_\odot \leq M \leq 0.8 M_\odot$	32
4.7c	Spatial distribution of F_r for $1.0 M_\odot \leq M \leq 1.55 M_\odot$	33
4.8	Efficiency factors as a function of spectral type	34
4.9	Magnetic energy density	35
4.10	Comparison with data from [23]	36

1 Introduction

Magnetic fields are ubiquitous in space. They can be observed in nearly all astronomical objects such as galaxies, interstellar clouds, stars, planets, etc. Although they are ubiquitous, the knowledge about their generation is quite small and comes at most from the analysis of our sun. It is believed that the magnetic fields in the celestial bodies we observe mainly come from electromagnetic processes called *dynamo effect*. The equations which lead these processes are well known but solving them is still very difficult and needs sophisticated dynamo simulations. Especially on this field huge progress has been made in the last decades. [4]

An important part in a comprehensive dynamo theory is a well-established scaling law which makes predictions about the magnetic field by calculating fundamental properties of the star or the region where dynamo is operating, respectively [5]. It would be a big step towards full understanding of the underlying processes of dynamo theory if a scaling theory was found which predicts magnetic field strengths for a wide range of celestial bodies. Good progress on this field was made by [8] who found a scaling law which was valid for planets as well as for low mass stars. The aim of this thesis is to evaluate if this law might also be valid for larger stars.

Within the last century huge efforts have been made in understanding stellar interiors (e.g. [14]). The growing computer power also supported this field since simulations of stellar structure got more and more sophisticated over the past 20 years. [14]

A relatively new, powerful method to study stellar interiors is given with the code suite *Modules for Experiments in Stellar Astrophysics* (MESA) which gives open source, robust, efficient, thread-safe libraries for a wide range of applications in computational stellar astrophysics. A key feature of this code suite is the model `MESA star` which is a one-dimensional stellar evolution code. The whole capabilities of MESA are described in [17–19].

In chapter 2 I explain the mechanisms of how stellar magnetic fields are produced

1 Introduction

and how the magnetic fields can be described by few quantities of a star according to different scaling laws.

In Chapter 3 I provide the methods how I approached the problem using the stellar evolution code `MESA star` and which parameters were used.

The results I obtained from this numerical approach are presented in chapter 4. I provide the quantities which are computed by the `MESA star` code as well as the magnetic energy densities which are computed according to the scaling law and compare these magnetic fields to data from observations collected in [23].

The results are discussed in chapter 5. The thesis is concluded in chapter 6.

2 Theoretical Foundations

In this chapter I present the fundamental equations and concepts to give a basic understanding where stellar magnetic fields come from and how they are structured. For this purpose I describe the mechanisms according to which stellar dynamos work, how the dynamo mechanisms in solar-like and cool stars differ and how rotational velocity influences the magnetic field strength in section 2.1. In section 2.2 I present the governing equations in Magnetohydrodynamics (MHD) and I introduce the most common dimensionless numbers which are used to describe the regimes in the stellar interiors and to control dynamo models. Section 2.3 treats different scaling laws for magnetic fields, how they are motivated and when they are applicable.

2.1 Stellar Dynamos

Stellar magnetic fields are mostly generated in convective zones of the star and result from complex mechanisms which occur in the moving plasma. These mechanisms are called *solar* (or in general *stellar*) *dynamo*. There is a good understanding how the dynamo in the Sun works since there are many data for this star, but anyhow it is difficult to measure magnetic fields from stars different than the Sun, therefore the generation processes of non solar-like stars are far from being understood. [23]

2.1.1 Convective zones of stars

The main difference in the structure of the Sun and cooler or hotter stars with respect to magnetic field generation is shown in figure 2.1. Stars of spectral type early-M, K, G and late-F have convective envelopes where the dynamo action takes place. Hotter stars (like A and B-stars) have a very thin or no outer convective zone, but a convective core which is larger for hotter stars. Cooler stars, like spectral type M3.5 and later are fully convective meaning that they lack the so called *tachocline*, the transition region between convective and radiative zone which is the place where

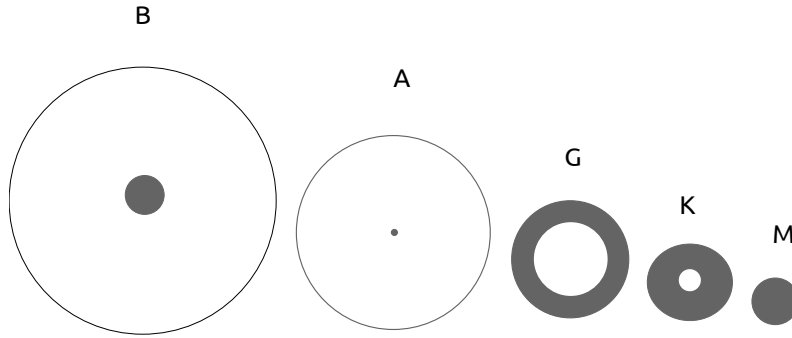


Figure 2.1: **Schematic representation of convective zones in stars**
 Grey regions represent convective, white regions radiative zones. The letter represents the spectral type. Neither star size nor size of convective zones are to scale. Graphic was made according to [4, p. 188].

stellar dynamo is supposed to be most efficient. For this reason the dynamo efficiency is expected to change dramatically between M3 and M4 stars.

Yet fully convective stars (i.e. stars with $M \leq 0.35M_{\odot}$) show stronger (by one order of magnitude) global magnetic fields than the Sun (e.g.[22]). This leads to the assumption that these stars have a different dynamo mechanism. [4, 8, 23]

2.1.2 α - and Ω -effect

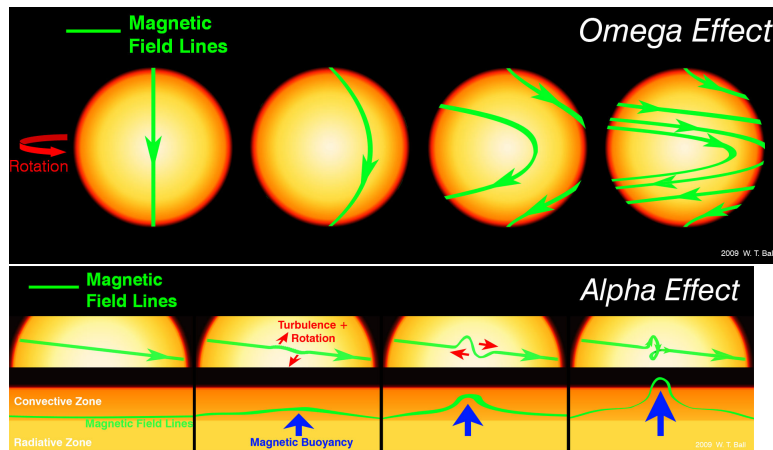


Figure 2.2: **Visualisation of Ω - and α -effect**
 For explanations see section 2.1.2. The graphic is taken from [2].

The process of field amplification is an interplay between convective motion and differential rotation. The originally *poloidal* (i.e. in the direction of the rotation axis, see figure 2.2, top, left) magnetic field is wind around the equator while the

flux lines are stretched and therefore strengthened. So, a *toroidal* field is produced. This process is called Ω -effect.

A toroidal field can be transformed into a poloidal field via the α -effect (figure 2.2, bottom). Due to convective and turbulent motions the flux lines rise upwards, twist and finally produce small scale poloidal fields. If the small scale fields connect, a large scale poloidal field can form. When those small scale *flux ropes* come to the surface the sunspots occur, i.e. areas on the surface which show a very high magnetic activity.

In stars with a tachocline, e.g. the Sun, a combination of the two effects provide dynamo action with the 11-year-long *solar cycle*, which means that magnetic activity of the star (measured by the number of sunspots) increases and decreases within a period of 22 years.

In planetary dynamos and dynamos of fully convective stars it is assumed that so called α^2 dynamos take place, which regenerate both the poloidal and toroidal magnetic fields entirely via the inductive action of small-scale turbulence as there are no shear flows which amplify the Ω -effect . [4, chapter 3.2]

2.1.3 Saturated fields

As sketched in section 2.1.2 rotation is essential for the function of the stellar dynamo, independent from the sort of the dynamo. A measure for the rotation time is the nondimensional Rossby number (2.15) (see section 2.2.2). [23] Observations show that the activity of stars saturate at low Rossby numbers (i.e. rotation periods which are small compared to convective timescales) [21].

Although magnetic flux and star activity are strongly connected (e.g. [15]) it is not clear from activity saturation that the magnetic flux also saturates. However through direct field measurements of M dwarfs there is evidence that the field saturates, too. [25]

2.2 Fundamental equations of Magnetohydrodynamics

When dealing with magnetic fields in stars, one has to be familiar with the science of electrically conducting fluids which induce magnetic fields. This field of study

which connects fluid dynamics and electromagnetism is called *magnetohydrodynamics* (MHD).

2.2.1 Basic set of equations

Induction equation. The electromagnetism is described by Maxwell's equations that can be written in differential form as (in SI units)

$$\nabla \cdot \mathbf{E} = \frac{\rho_e}{\epsilon_0} \quad (2.1)$$

$$\nabla \times \mathbf{E} = -\frac{\partial \mathbf{B}}{\partial t} \quad (2.2)$$

$$\nabla \cdot \mathbf{B} = 0 \quad (2.3)$$

$$\nabla \times \mathbf{B} = \mu_0 \mathbf{J} + \mu_0 \epsilon_0 \frac{\partial \mathbf{E}}{\partial t}. \quad (2.4)$$

In equation (2.4) the displacement current $\frac{\partial \mathbf{E}}{\partial t}$ can be ignored if the velocities are non-relativistic, therefore equation (2.4) reduces to

$$\nabla \times \mathbf{B} = \mu_0 \mathbf{J}. \quad (2.5)$$

Together with Ohm's law

$$\mathbf{J} = \sigma(\mathbf{E} + \mathbf{u} \times \mathbf{B}) \quad (2.6)$$

and equation (2.2) this yields the magnetohydrodynamic *induction equation*

$$\frac{\partial \mathbf{B}}{\partial t} = \nabla \times (\mathbf{u} \times \mathbf{B} - \eta \nabla \times \mathbf{B}) \quad (2.7)$$

with $\eta = \frac{1}{\mu_0 \sigma}$, the magnetic diffusivity. The induction equation describes the behavior of the magnetic field. The terms on the RHS denote the induction of the moving fluid and the dissipation of the currents which sustain the field. [4, chapter 1.3]

Equation of motion. The base for the equation of motion is the *Navier-Stokes* equation

$$\frac{D\mathbf{u}}{Dt} = -\frac{1}{\rho} \nabla p + \frac{1}{\rho} \nabla \cdot \boldsymbol{\epsilon}, \quad (2.8)$$

where the operator $\frac{D}{Dt}$ denotes the *Lagrangian derivative* $\frac{\partial}{\partial t} + \mathbf{u} \cdot \nabla$, which is the variation alongside the moving fluid elements. ϵ is the *viscuos stress tensor* which describes the viscous forces acting on a fluid element.

The other forces which also act on the fluid element are added to the RHS of equation (2.8), namely Coriolis force (if the equation is written down in a reference frame moving with the rotating star), buoyancy force and Lorentz force, so that the equation is

$$\frac{D\mathbf{u}}{Dt} = \frac{\partial\mathbf{u}}{\partial t} + (\mathbf{u} \cdot \nabla)\mathbf{u} = -\frac{1}{\rho}\nabla p - 2\boldsymbol{\Omega} \times \mathbf{u} + \alpha\Delta T\mathbf{g} + \frac{1}{\rho}(\mathbf{J} \times \mathbf{B}) + \frac{1}{\rho}\nabla \cdot \epsilon. \quad (2.9)$$

The Lorentz force $\mathbf{J} \times \mathbf{B}$ is taken in its *MHD approximation*, where electrostatic forces are neglected. [4, chapter 1.2]

2.2.2 Nondimensional numbers

In order to describe the equations from section 2.2.1 in a nondimensional form, there are several nondimensional parameters which represent ratios of quantities appearing in these equations, i.e. forces in the equation of motion (2.9) and the induction equation (2.7). Here I present the most important of those numbers which are used in dynamo models as input and control parameters. [6, 11]

The magnetic Reynolds number

$$Rm = \frac{ul_{\text{mag}}}{\eta} \quad (2.10)$$

is the ratio between magnetic induction and dissipation. It must be large enough for a dynamo to be self-sustained. According to dynamo models the critical value is about 50 [6]. l_{mag} is a characteristic length scale for the magnetic field.

The Elsasser number

$$\Lambda = \frac{\sigma B^2}{2\rho\Omega}, \quad (2.11)$$

describes the ratio between Lorentz and Coriolis force. It is used for scaling laws (see section 2.3.1), since the two forces are assumed to be equal in magnetostrophic force balance and therefore Λ should be one. In dynamo models the Elsasser number

2 Theoretical Foundations

was in the range between 0.06 and 100 [6], therefore this number might not be a good measure for the degree of force balance.

The Prandtl number

$$Pr = \frac{\nu}{\kappa} \quad (2.12)$$

and the magnetic Prandtl number

$$Pm = \frac{\nu}{\eta} \quad (2.13)$$

describe the relation of viscosities. The Prandtl numbers serve as control parameters for dynamo models and are usually set to one but can vary by about one order of magnitude if the Ekman number $E = \frac{\nu}{\Omega l^2}$ is adapted.[6]

The Rayleigh number

$$Ra = \frac{\alpha \Delta T g l_c^3}{\nu \kappa} \quad (2.14)$$

which measures the ratio between buoyancy and viscous forces must be high enough for convective motions to occur [35]. l_c is the typical size of the convective structure in the celestial body (i.e. the planet or star).

The Rossby number

$$Ro = \frac{1}{\Omega \tau_c}, \quad (2.15)$$

where τ_c is the *convective overturn time*, i.e. the time scale for convective motions [12]. This number measures the importance of inertial forces and is a measure for the magnetic activity of the star, i.e. the activity and magnetic field rise with decreasing Ro . [23]

2.3 Scaling laws for the magnetic fields of planets and stars

There have been multiple attempts to describe the magnetic field of planets and stars with a *scaling law*, which means that the magnetic field is approximated by some basic properties of the planet or the star, respectively.

When data first showed magnetic fields in planets, also the first scaling laws were proposed, e.g. the empirical *magnetic Bode Law* which assumes a dependency between magnetic moment and angular momentum [27].

2.3.1 Elsasser number rule

More sophisticated scaling laws assume magnetostrophic force balances of the terms in equation (2.9). A very basic scaling law is the *Elsasser number rule* assuming that the Elsasser number Λ (2.11) is of the order of one leading to the scaling law [32]

$$B^2 \propto \frac{\rho\Omega}{\sigma}. \quad (2.16)$$

The theoretical foundation for this is that rotation or magnetic field alone inhibit convection, but the combination of the two effects would enhance the magnetic field, therefore the two forces should be in a balance and Λ equilibrates at around one. However – as mentioned in section 2.2.2 – dynamo models showed that Λ is varying with input parameters such as Rm or E which is why the scaling law (2.16) might not hold in general.

2.3.2 Energy flux scaling

Besides magnetostrophic force balance there are also scaling laws based on thermodynamic considerations, in particular the amount of ohmic dissipation $D = \mathbf{J} \cdot \mathbf{J}/\sigma$ as a fraction of the available heat flux per unit volume, which is q_c/H_T . With equation (2.5) the ohmic dissipation becomes $D = (\nabla \times \mathbf{B})^2/(\mu_0^2\sigma) \propto 2\eta E_{\text{mag}}/l_{\text{mag}}^2$ [7]. Therefore the magnetic energy density scales as

$$E_{\text{mag}} = \frac{B^2}{2\mu_0} \propto f_{\text{ohm}} \frac{l_{\text{mag}}^2}{2\eta} \frac{q_c}{H_T}, \quad (2.17)$$

2 Theoretical Foundations

where f_{ohm} is the fraction of ohmic dissipation to available convected heat flux. l_{mag} refers to the length scale on which variations of the magnetic field strength take place. $l_{\text{mag}}^2/2\eta$ is proportional to the dissipation time τ_η . [7] found out that τ_η scales with the inverse of the magnetic Reynolds number Rm from equation (2.10), i.e. $\tau_\eta \propto l_{\text{mag}}^2/\eta Rm = l_{\text{mag}}/u$. Together this yields the scaling law

$$\frac{B^2}{2\mu_0} = cf_{\text{ohm}} \frac{l_{\text{mag}}}{u} \frac{q_c}{H_T}. \quad (2.18)$$

For u there are several scaling rules, based on different mechanisms. The first rule is based on the magnetostrophic force balance between Coriolis and buoyancy force, i.e. the second and third term on the RHS of equation (2.9), therefore

$$\alpha g \Delta T \propto \Omega u. \quad (2.19)$$

The convected heat flux which is transported due to temperature differences ΔT can be written as

$$q_c \propto \rho c_p u \Delta T, \quad (2.20)$$

therefore replacing ΔT in (2.19) and introducing the temperature scale height

$$H_T = c_p/\alpha g \quad (2.21)$$

for the temperature scale height the convective velocity scales as [31]

$$u = \left(\frac{q_c}{\Omega \rho H_T} \right)^{1/2}. \quad (2.22)$$

The second rule considered here is based on the mixing length theory (section 3.1). Balancing the nonlinear inertia term (second term of the Lagrangian derivative on the LHS from equation (2.9)) with the buoyancy term (third term on RHS of (2.9)) and assuming the mixing length l_m for the length scale of the spatial derivatives of the inertia term yields $u^2/l_m \propto \alpha g \Delta T$ which together with equations (2.20) and (2.21) leads to the velocity scaling rule

$$u = \left(\frac{q_c l_m}{H_T \rho} \right)^{1/3}. \quad (2.23)$$

2.3 Scaling laws for the magnetic fields of planets and stars

These two velocity scaling rules together with the scaling rule (2.18) yield the two scaling laws [31]

$$\frac{B^2}{2\mu_0} \propto l_{\text{mag}} f_{\text{ohm}} \left(\frac{\Omega \rho q_c}{H_T} \right)^{1/2} \quad (2.24)$$

for velocity scaling according to equation (2.22) and [6]

$$\boxed{\frac{B^2}{2\mu_0} \propto f_{\text{ohm}} \left(q_c \frac{l_{\text{mag}}}{H_T} \right)^{2/3} \rho^{1/3}}, \quad (2.25)$$

respectively.

Since the quantities in equation (2.25) change within the radius of the dynamo an efficiency factor F is introduced via averaging the varying quantities over the convective zone [8]. This efficiency factor is given by

$$F^{2/3} = \frac{1}{V} \int_{r_i}^R \left(\frac{q_c(r) l_{\text{mag}}(r)}{q_0 H_T(r)} \right)^{2/3} \left(\frac{\rho(r)}{\langle \rho \rangle} \right)^{1/3} 4\pi r^2 dr, \quad (2.26)$$

where r_i denotes the inner radius of the dynamo region (in stars the inner radius of the convective envelope, if there is one), V the volume of the dynamo region, q_0 some reference flux for which the total energy flux at the outer boundary of the star is taken and $\langle \rho \rangle$ the average density over the dynamo region. A usual value for the length scale l_{mag} is the pressure or density scale height H_p or H_ρ , respectively.

The scaling law (2.25) becomes then

$$\frac{\langle B^2 \rangle}{2\mu_0} = c \langle \rho \rangle^{1/3} (F q_0)^{2/3}, \quad (2.27)$$

where c is a constant. [5]

2.3.3 Application of energy flux scaling to stars

The scaling law (2.25) was also applied to stars [8]. The results of this application are shown in figure 2.3.3. As follows from equation (2.25) the scaling law is independent of both the electrical conductivity (and therefore magnetic diffusivity) and the rotation rate. This doesn't mean that these parameters are completely unimportant but they have to be in the right regime for the dynamo to work. According to (2.10)

the diffusivity must be low enough for Rm to be supercritical and Ω must be large in comparison to $1/\tau_c$ so that the Rossby number (2.15) is in a regime where the field is saturated.

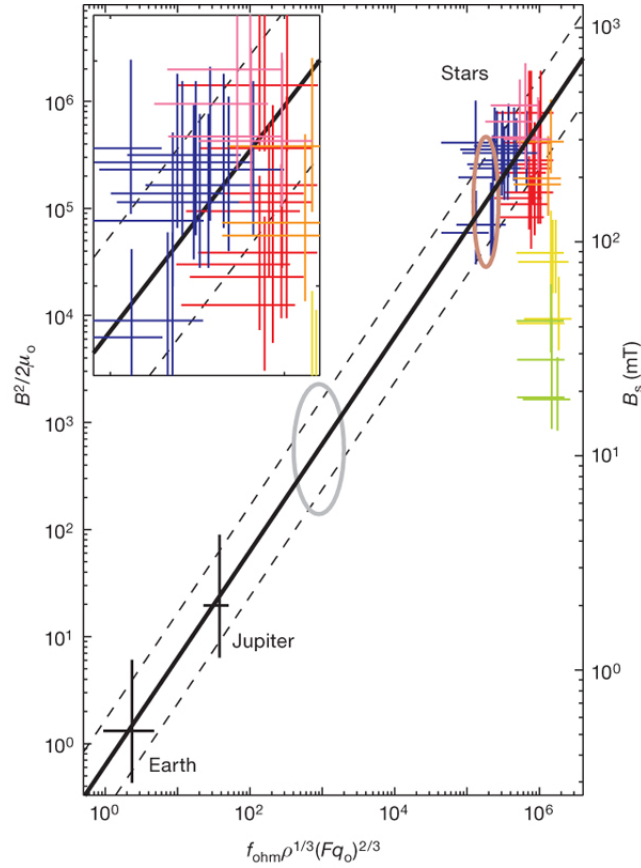


Figure 2.3: **Scaling law (2.25) applied to Earth, Jupiter and stars**

The scale on the LHS shows magnetic energy density. The scale on the RHS shows the measured r.m.s. field strength at the dynamo surface. For Earth and Jupiter the value F is calculated based on estimations of the heat flux in the interior. For stars $F = 1$ is assumed. Blue, red and pink denote different cool stars (T Tauri and M stars), stars of 0.6 - 1.1 solar masses are shown in green for rotation periods $P > 10$ d, yellow for $4 \text{ d} < P < 10 \text{ d}$ and orange for $P < 4 \text{ d}$. The graphic is taken from [8].

3 Numerical approach

In this chapter I describe the procedure how convection is treated via the *mixing-length theory* (section 3.1), how the stellar evolution code `MESA star` works (section 3.2), how the magnetic energy densities according to equations (2.25)-(2.26) are calculated (section 3.3) and how I varied parameters (section 3.4).

3.1 Mixing-length theory of convection

Energy transport by convection means that macroscopic mass elements (*convective elements*) are transported from hotter to cooler regions because of differences in density. The hot elements cool down and thereby release their heat to the surrounding. This process can be very efficient in stellar interiors due to the high density.

Due to the turbulent motions in stellar interiors it is very difficult to treat convection in a theoretical way. There have been made large efforts in solving the underlying hydrodynamical equations but still these numerical simulations are limited to certain time scales and only thin convection zones.

With the so called *mixing-length theory* by Ludwig Prandtl a theory exists which provides a simple method for treating convection locally. The theory has been tested with a three-dimensional numerical simulation of efficient convection which support the validity of the assumptions the theory makes [3]. Empirical tests also show good agreement of stellar models resulting from this theory with observations.

In a basic picture the theory is equivalent to molecular heat transfer where the analogon to molecules are the convective elements and the analogon to the mean free path is the *mixing length* l_m . After the mixing-length the convective element mixes with the surrounding. The advantage of this theory is that the only free parameter is l_m which is usually assumed to be in the order of the pressure scale height H_P . To be more precise, the parameter which is needed is the *mixing length parameter*

3 Numerical approach

α_{MLT} , defined by

$$l_m = \alpha_{\text{MLT}} H_P. \quad (3.1)$$

α_{MLT} is assumed to be of the order of 1. More reasonable values are obtained by comparison of the effective temperature or radius of stellar models with observed stars. From this method values between 1.5 and 2.0 are obtained. [14, chapter 7]

[10] present an empirical calibration of α_{MLT} according to which it takes values between 1.86 and 2.17 depending on calibration stars and assumed stellar metallicity.

3.2 MESA – Modules for Experiments in Stellar Astrophysics

Modules for Experiments in Stellar Astrophysics (MESA) provides libraries for a wide range of applications in stellar astrophysics. These libraries are independent from each other and each library provides different aspects of the numerics and physics which are necessary to compute models for stellar physics. `MESA star` is a stellar evolution code which combines the capabilities of most of these modules in order to solve the structure and composition equations in the interior of stars. [17] The procedure how `MESA star` computes quantities inside the star are described in [17]:

[It] first reads the input files and initializes the physics modules to create a nuclear reaction network and access the EOS and opacity data. The specified starting model [...] is then loaded into memory, and the evolution loop is entered.

The procedure for one timestep has four basic elements. First, it prepares to take a new timestep by remeshing the model if necessary. Second, it adjusts the model to reflect mass loss by winds or mass gain from accretion, adjusts abundances for element diffusion, determines the convective diffusion coefficients, and solves for the new structure and composition using the Newton-Raphson solver. Third, the next timestep is estimated. Fourth, output files are generated.

3.3 Calculation of quantities

My analysis basically consisted of two parts: the computation of stellar properties via `MESA star` and the calculation of the desired properties according to section 2.3.

Computation of stellar properties. In a first step I prepared the computation by giving input parameters for stellar mass, age, and mixing-length parameter. The actual choice of these input parameters is described in section 3.4.

`MESA star` then computes stellar properties for every star according to the procedure described in section 3.2 and writes them into output files which are used in further analysis.

The quantities which are important in my study are listed in table 3.1.

Quantity	Symbol
Bolometric luminosity	L
Convective velocity	v_c
Ratio of convective luminosity to bolometric Luminosity	$\frac{L_c}{L}$
Gravitational acceleration	g
Pressure scale height	H_p
Mass of shell	dm
Radius	r
Temperature	T
Pressure	p
Specific heat capacity	c_p
Density	ρ
Shell thickness	dr
Effective temperature	T_{eff}

Table 3.1: **List of quantities provided by `MESA star`**

Listed are the quantities which are needed in the analysis. The quantities above the lower doubled line are spatial varying quantities, the quantity below is a value which characterizes the model.

Calculation of desired quantities. The analysis of the data provided by `MESA star` in order to test the scaling law (2.25) is done with `python`. The analysis consists of four parts: reading data, preparation, integration, and output.

In a first step stellar structure is read from the `MESA star` output for every mass-age- α_{MLT} combination and stored into arrays. Some of these provided quantities are shown in section 4.1.

3 Numerical approach

The second step is the calculation of convection zone depths since the integration in equation 2.26 only takes place in this zone. The convective zone is defined as the regime where the convective flux (and therefore also the convective luminosity $L_c = q_c 4\pi r^2$) is nonzero. In low-mass stars ($M < 3.5M_\odot$) this is the whole star, in higher mass stars the number of the shell where the convective luminosity vanishes has to be found.

In a next step several quantities which are not directly provided are calculated. The first quantity is the temperature gradient $\frac{\partial T}{\partial r}$ which is calculated via derivation of the $T(r)$ data from `MESA star`. The second is the temperature scale height which makes use of the temperature gradient and is calculated via the equation

$$H_T = T \left| \frac{\partial T}{\partial r} \right|^{-1}. \quad (3.2)$$

The density scale height is calculated via H_P and H_T according to the equation [34]

$$H_\rho = \frac{1}{\frac{1}{H_T} + \frac{1}{H_P}}. \quad (3.3)$$

The next step is the calculation of the integrand in equation (2.26),

$$F_r(r) = \left(\frac{q_c(r)}{q_0} \frac{l_{\text{mag}}(r)}{H_T(r)} \right)^{2/3} \left(\frac{\rho(r)}{\langle \rho \rangle} \right)^{1/3} \quad (3.4)$$

for every star layer. As proposed in [8] I took H_ρ as typical length scale l_{mag} . The average density $\langle \rho \rangle$ was computed by dividing the mass of the convective volume $M_c = \int_{r_i}^R dm$ by its volume $V_c = \frac{4\pi}{3}(R^3 - r_i^3)$. Since L_c was provided instead of q_c , the equation (3.4) becomes

$$F_r(r) = \left(\frac{L_c(r)}{L(R)} \frac{R^2}{r^2} \frac{H_\rho(r)}{H_T(r)} \right)^{2/3} \left(\frac{\rho(r) \frac{4\pi}{3}(R^3 - r_i^3)}{\int_{r_i}^R dm} \right)^{1/3}. \quad (3.5)$$

The factor F is then obtained by calculating (cf. equation (2.26))

$$F = \left(\frac{3}{4\pi(R^3 - r_i^3)} \int_{r_i}^R F_r(r) 4\pi r^2 dr \right)^{3/2} \quad (3.6)$$

for every star (i.e. mass-age- α_{MLT} combination). According to equation (2.27) the mean magnetic energy densities at the dynamo surface are calculated in the next

step and $F_r(r)$, F and $E_{\text{mag}} = \frac{B^2}{2\mu_0}$ are stored for every star for further analysis.

3.4 Choice of parameters

The mass range of my analysis covered the range from M6 stars ($0.1 M_\odot$) to F0 stars ($1.55 M_\odot$). For every model I computed 9 different ages from 1×10^6 yrs to 1×10^{10} yrs.

Since it is not well known which α_{MLT} is appropriate (cf. section 3.1) I used a range from 1.6 to 2.4 for this value.

Table 3.2 provides a list of assumed values for mass, age, and mixing-length parameter.

$M [M_\odot]$						age [yrs]		α_{MLT}
0.1	0.11	0.12	0.13	0.15	0.19	1×10^6	3×10^6	1.6
0.2	0.22	0.25	0.27	0.3	0.35	1×10^7	3×10^7	1.8
0.4	0.5	0.6	0.7	0.8	0.9	1×10^8	3×10^8	2.0
1.0	1.1	1.2	1.3	1.4	1.5	1×10^9	3×10^9	2.2
1.55						1×10^{10}		2.4

Table 3.2: **List of parameters used in the analysis**

4 Results

In this chapter I present the results from the computations made as described in chapter 3.

First, in section 4.1 the quantities are shown as a function of radius which were directly computed by MESA, namely temperature T , the ratio of convective energy flux to bolometric flux q_c/q_0 , and density ρ . Besides, the energy flux at the outer boundary of the star and the average densities of convection zones are shown for different models.

In section 4.2 the radial dependencies of the efficiency factors according to equation (3.5) and in section (4.3) the magnetic energy densities according to formula (3.6) as a function of mass and age of the star as well as a function of spectral type are shown .

In section 4.4 I compare the results with data collected in [23].

4.1 Provided quantities

4.1.1 Radial Profiles

Temperature

Figure 4.2 shows various temperature profiles for stars with different masses and computed with different values for α_{MLT} . Variations in the mixing length parameter are hardly visible in these plots.

Variations in age do change the temperature profile in a quantitative way, i.e. the temperatures are higher for older stars (the variation is about 10% in the core and less in the outer regions). This difference is more visible for lower mass stars, i.e. M stars.

The mass of the star has more influence onto the temperature profile. In principle the temperature is higher for higher mass stars but the profile also changes qualitatively. While for M dwarfs the decrease of temperature is more or less linear, it is

4 Results

exponentially for stars with $M \gtrsim 1.0M_{\odot}$.

I also provided the effective temperatures T_{eff} which are used to assign the models to spectral types. The T_{eff} ranges for certain mass ranges are provided in table 4.1.

Convective energy flux

The energy flux profiles are shown in figure 4.3. I discriminate two qualitatively different types: fully and partially convective stars (cf. section 2.1.1). The MESA star results confirm the results that stars with $M \leq 0.35M_{\odot}$ are fully convective and larger stars have a convective envelope.

The ratio of convective zone width to star radius decreases with increasing mass and increases with increasing age.

In stars with convective envelope there is also a convective core whose flux decreases with increasing age and decreasing mass. Since the magnetic field produced in the convective cores is shielded by the radiative zone I neglect the convective cores in the integration. Therefore the convective cores are not shown.

The mixing-length parameter α_{MLT} influences the convection zone widths of stars: increasing α_{MLT} means deeper convection zones. For fully convective stars or stars with deep convective envelopes ($r_i/R < 0.7$) the mixing-length parameter has almost no influence.

Density

The density profiles in the convective zones of the star (where convective energy flux according to figure 4.3 is not zero) are shown in figure 4.4.

Strong variations in the order of magnitude are visible. This is due to the fact that for high mass stars with thin convective envelopes only the outer zone of the star where density is low is shown.

The α_{MLT} dependency is rather weak for low mass stars, for stars with $M \geq 1.0M_{\odot}$, where the density variation over the thin convective envelope is shown, the influence of the mixing-length parameter is stronger.

4.1.2 Overall values

Total energy flux

Figure 4.5 shows the temporal variation of energy flux, i.e. $L/4\pi R^2$ at three different mixing-length parameters for different masses. It is visible that the flux increases

with increasing mass. The difference in flux between the lowest and the highest mass stars in my study is about two orders of magnitude. The age of the star and the mixing-length parameter do not have such a big influence as the flux is in the same order of magnitude over the whole range. It differs by a maximum of 30 % in the ages-range (for $1.5 M_{\odot}$) and a maximum of 20 % in the α_{MLT} -range (for $1.0 M_{\odot}$).

Average Density

Figure 4.6 shows the temporal evolution of average density of the convective zone of the stars at three different mixing-length parameters. The average density in the convective zone decreases with higher masses. This is due to the fact that the convective zone shrinks and the density is lower in the outer regions of the star (cf. figure 4.4).

The age has an influence in the average density. For the low mass stars the difference (about 50 % difference over the whole age-range for $0.1 M_{\odot}$) occurs because the star contracts with age. The mixing-length parameter has basically no influence for those stars. For higher mass, i.e. partially convective stars, the difference in age (about 90 % difference for $1.5 M_{\odot}$) and mixing-length parameter (about two orders of magnitude difference for $1.5 M_{\odot}$) occur because the convection zone width differs with those two quantities (cf. figure 4.3).

4.2 Spatial distribution of efficiency factor

Figures 4.7a-4.7c show the spatial distribution of the integrand in efficiency factor F_r according to equation (3.5) for $\alpha_{\text{MLT}} = 2.0$. As shown in section 4.1 the influence by the mixing-length parameter is less important than the influence of mass and age which is why these plots are shown for an intermediate value. Also shown are the integrated values for the efficiency factor F . For the other mixing-length parameters the plots do not differ in qualitative way.

One can observe that every star in figure 4.7a (i.e. stars with $M < 0.3 M_{\odot}$) has a nonzero magnetic energy density for its whole r -range which means that it is fully convective (cf. section 4.1.1).

Furthermore one can observe that the magnetic fields in fully convective stars and in the outer convective zones of partially convective stars behave similar: they increase until they reach a maximum within the inner region of their convective zones and then decrease monotonically until they reach zero at the outer boundaries.

4 Results

One observes that the oldest stars of $M = 0.35 M_{\odot}$ are still fully convective but have a minimum at about $0.3 R_{\text{star}}$.

Moreover for stars with $M \geq 0.35 M_{\odot}$ convective cores can be observed which always vanish at ages of 10^{10} years but do not shrink monotonously. If any magnetic field was produced inside these convective cores it would be shielded by the radiation zone between convective core and convective envelope and therefore it is not visible at the surface. For this reason I neglected these region for the integration.

The integrated efficiency factors for fully convective stars are in the range between 0.27 (for $0.35 M_{\odot}$ and 10^9 years) and 0.43 ($0.1 M_{\odot}$ and 10^9 years) and for stars with convective envelopes in the range between 0.1 ($1.5 M_{\odot}$ and 10^7 years) and 0.35 ($1.5 M_{\odot}$ and 10^{10} years). While the efficiency factors decrease rapidly with higher masses at low ages, they increase for $M \gtrsim 1.0 M_{\odot}$ with mass for higher ages ($\gtrsim 10^9$ years).

4.3 Magnetic Energy Densities

The assignment of star models to spectral types is done via the effective temperature of the star as provided by `MESA star`. Figure 4.1 shows the calibration I used which temperature is assigned to which spectral type according to [13]. The assignment which masses are assigned to which spectral tpe is shown in table 4.1.

Mass range [M_{\odot}]	T_{eff} range [K]	spectral types
0.1 – 0.12	3089 – 3268	M6, M5
0.13 – 0.15	3308 – 3491	M5, M4, M3
0.19 – 0.27	3569 – 3670	M3, M2
0.3 – 0.6	3675 – 4057	M2, M1, M0
0.7 – 0.8	4293 – 5134	K6, K5, K3, K2, K1
0.9 – 1.1	5150 – 6131	K1, K0, G9 – G0, F9
1.2 – 1.55	5995 – 7361	G1, G0, F9 – F0

Table 4.1: **Assignment of spectral types to masses**

The assignment of effective temperatures T_{eff} to spectral types is done according to the calibration used in [13] (cf. figure 4.2). The range in T_{eff} are minimum and maximum effective temperature in the respective mass range over the whole age- and mixing-length parameter range.

In figure 4.8 the integrated efficiency factors are shown as a function of spectral type. The range in the y -values represent the range of different magnetic field strengths assigned to the same spectral type.

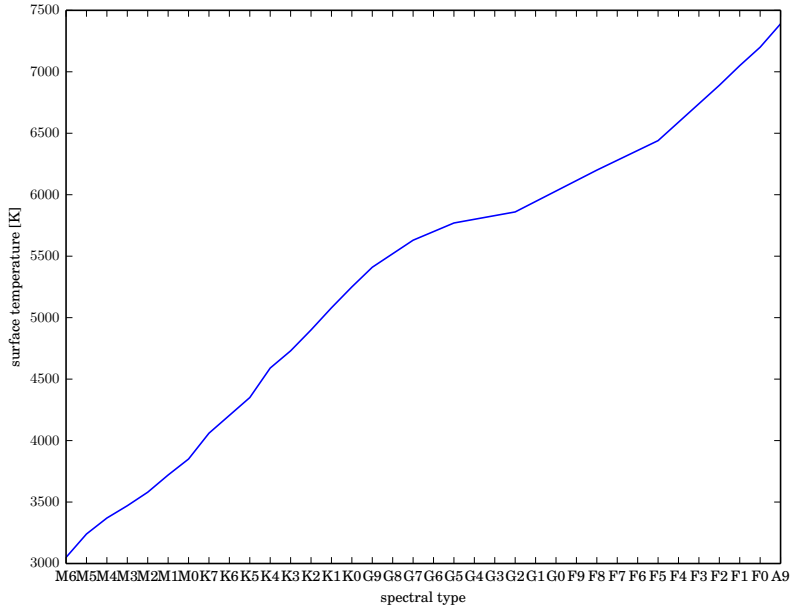


Figure 4.1: **Calibration of spectral types**
The calibration is taken from [13].

It is visible that the efficiency factors F basically all are in the range between 0.1 and 0.5 and the late type stars have larger values than the early type stars. This supports the observations from section 4.2. Only for early F stars the efficiency factor decreases below 0.1 (cf. figure 4.7c, $1.55 M_{\odot}$).

Figure 4.9 shows how the obtained magnetic energy densities according to equation 2.25 behave, in the upper plot as a function of spectral type and in the lower plot as a function of mass for different ages and α_{MLT} . In the lower plot a young, an intermediate, and an old age as well as two intermediate mixing-length parameters are shown.

It is visible that the energy densities are higher for low mass, i.e. fully convective stars ($M < 0.35 M_{\odot}$, spectral type M1), and decrease for higher masses. The maximum magnetic energy density which is reached in this study is 0.81 MJ/m^3 for $M = 0.15 M_{\odot}$, 10^{10} years and $\alpha_{\text{MLT}} = 2.4$ (spectral type M3). For high mass stars ($M \geq 0.6 M_{\odot}$) the maximum magnetic energy density is 0.28 MJ/m^3 for $M = 0.9 M_{\odot}$, 3×10^8 years and $\alpha_{\text{MLT}} = 2.4$ (spectral type K0).

4.4 Comparison with Observations

4.4.1 Measuring stellar magnetic fields

Stellar magnetic fields are measured by observation of the splitting of absorption lines due to the Zeeman effect. There are several problems in measuring magnetic fields. The major ones are discussed here.

One issue is that in cool stars most of the absorption lines are molecular lines. Those molecular lines are mostly weakly sensitive to magnetic fields. However some of them, like the diatomic molecules FeH and CrH, are sensitive but the so called *Landé g-factors*, which are measures for the sensitivity to magnetic fields, are poorly known for molecular lines. [9, 23]

Another issue is the fact that low mass stars are very faint which is why large telescopes are needed in order to obtain detailed spectra for those stars. In contrary, high mass stars are brighter but their magnetic fields are weak and therefore broadening mechanisms due to turbulence and rotational effects become important.

Since the scaling law doesn't account for the geometry of the field I compared the obtained fields with the unpolarized integrated flux measurements Bf (the so called *Stokes I* component of the field) where the so called *filling factor* f is the ratio of the surface which is covered by starspots.

4.4.2 Comparison

Figure 4.10 shows a comparison of the computation with data for the magnetic flux Bf at the stellar surface which are published in [1, 16, 20, 22, 24, 26, 28–30, 33] and collected in [23]. The assignment of star models to spectral types is done via the effective temperature of the star as provided by `MESA star` (cf. figure 4.2). The x -errorbars account for the fact that star models with different magnetic fields are assigned to the same spectral types. Errors for y -values are obtained from published data if given. If no positive but negative error is given, the value is an upper bound for the field.

The blue line describes the correlation between scaling law and data if $B/B_s = 3.5$ is assumed, i.e. a factor of $\frac{1}{3.5}$ of the produced magnetic field is visible at the surface. [8]

With that assumption the scaling law fits within one order of magnitude. It is visible that magnetic fields of early type stars are lower than those of late type

stars but still in a comparable range. The magnetic field measurements of most of the early type stars are lower compared with the scaling law (spectral type K, G and F). This is due to the fact that they are mostly slow rotators for which the scaling law is not applicable (cf. section 2.3.3). As described in section 4.4.1 it is difficult to observe magnetic fields in fast rotating high mass stars since the rotational broadening becomes important.

4 Results

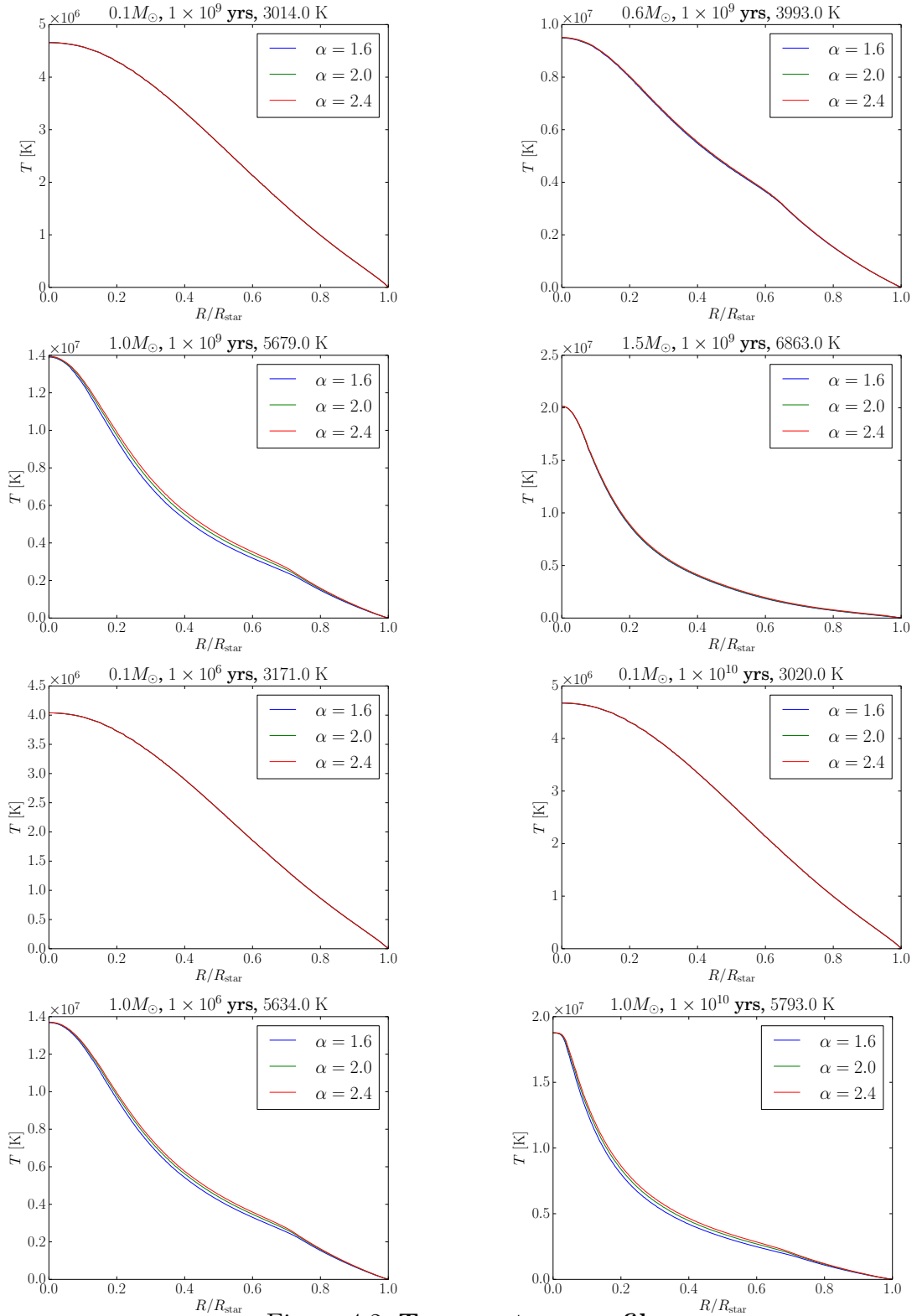


Figure 4.2: Temperature profiles

The upper two rows show the variation in mass at the same age, the lower two rows show the difference in age at the same mass for two different masses. The profiles are shown for three different mixing-length parameters. The title provides mass and age of the star as well as the effective temperature for $\alpha_{\text{MLT}} = 2.0$.

4.4 Comparison with Observations

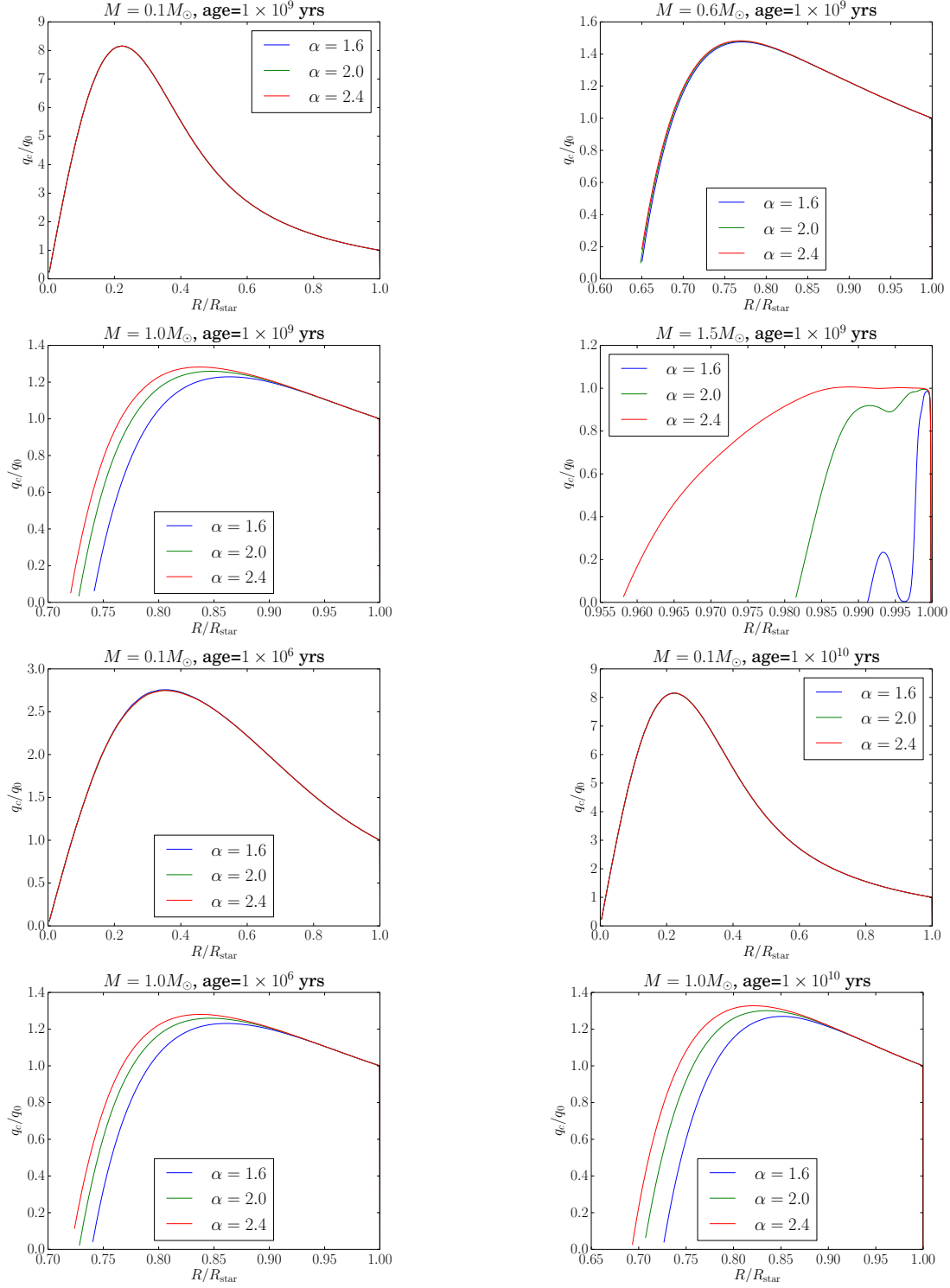


Figure 4.3: Convective energy fluxes

The fluxes are normalized by the flux at the outer boundary of the star. The upper two rows show the variation in mass at the same age, the lower two rows show the difference in age at the same mass for two different masses. The profiles are shown for three different mixing-length parameters. For partially convective stars only the convective envelope is shown as the flux in the core is higher than in the envelope (because of the r^{-2} -dependency of the flux) and therefore distorts the plot (cf. figure 4.7c, where insets are needed to compare the convective envelopes).

4 Results

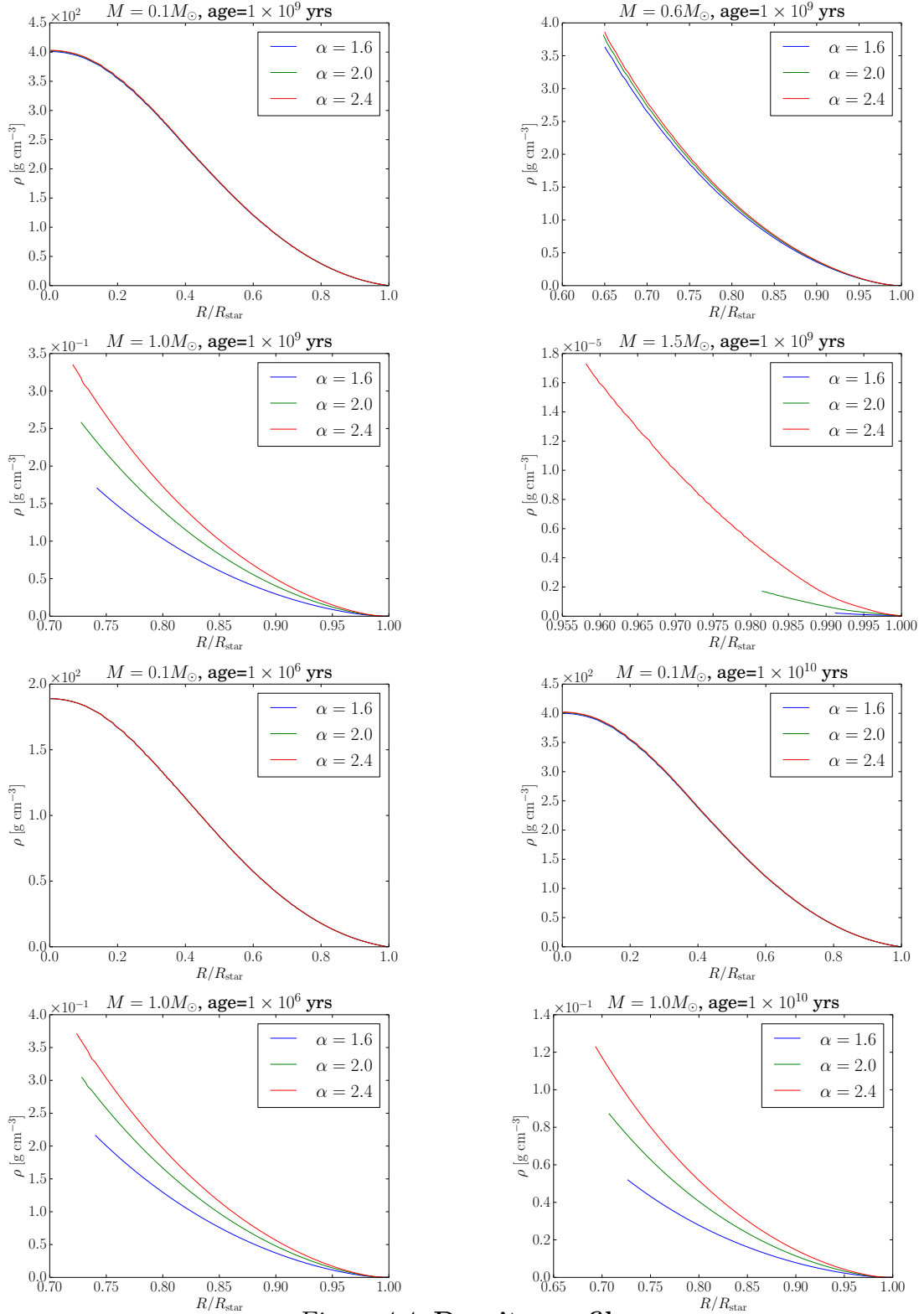


Figure 4.4: Density profiles

The upper two rows show the variation in mass at the same age, the lower two rows show the difference in age at the same mass for two different masses. The profiles are shown for three different mixing-length parameters. For partially convective stars only the convective envelopes are shown.

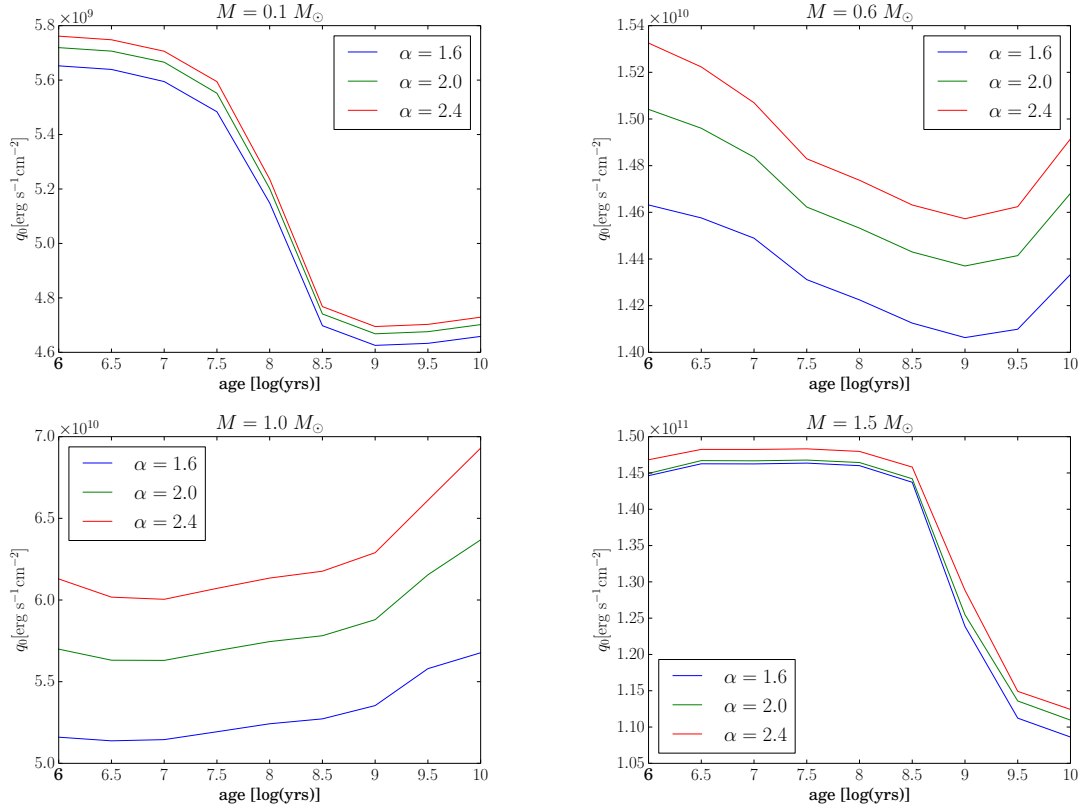


Figure 4.5: **Energy flux at the outer boundary**

The flux is calculated with the luminosity via $q_0 = L_0/4\pi R^2$ where L_0 is the luminosity at the outer boundary of the star.

4 Results

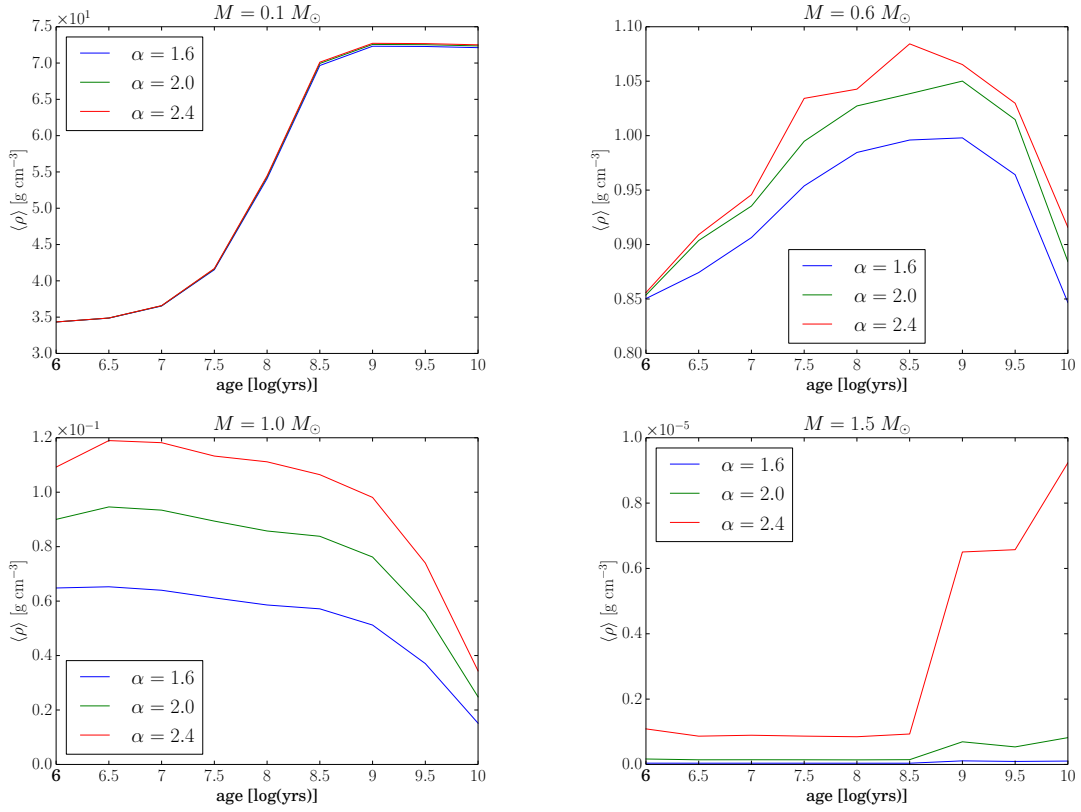


Figure 4.6: Average density

The average is taken over the convective envelope if the star is partially convective.

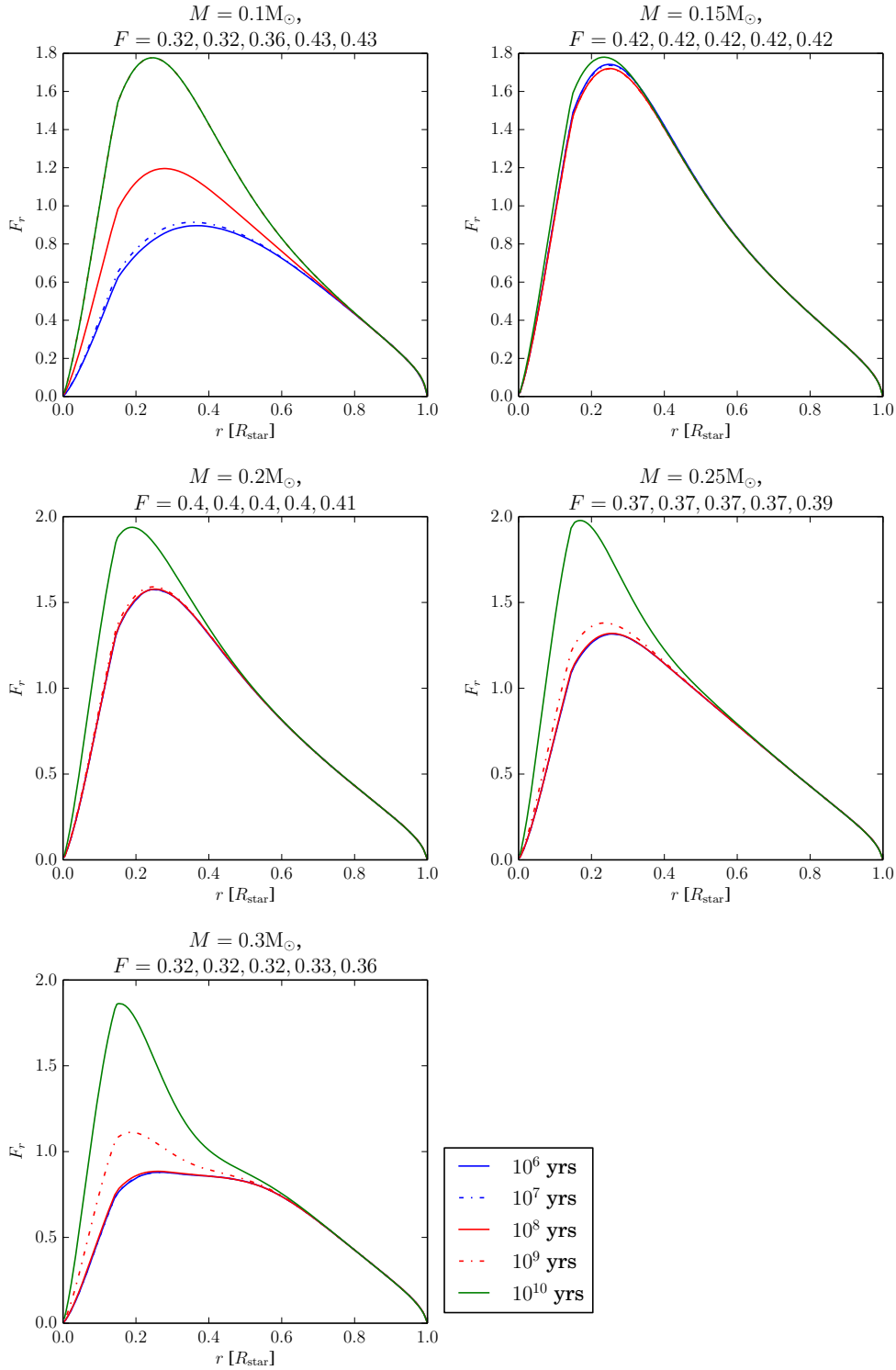


Figure 4.7a: **Spatial distribution of F_r for $0.1 M_\odot \leq M \leq 0.3 M_\odot$**
 The value F_r is calculated according to equation 3.5. The values for F in the title are integrated values according to equation (3.6) for the ages 10^6 , 10^7 , 10^8 , 10^9 and 10^{10} years. The mixing-length parameter is $\alpha_{\text{MLT}} = 2.0$.

4 Results

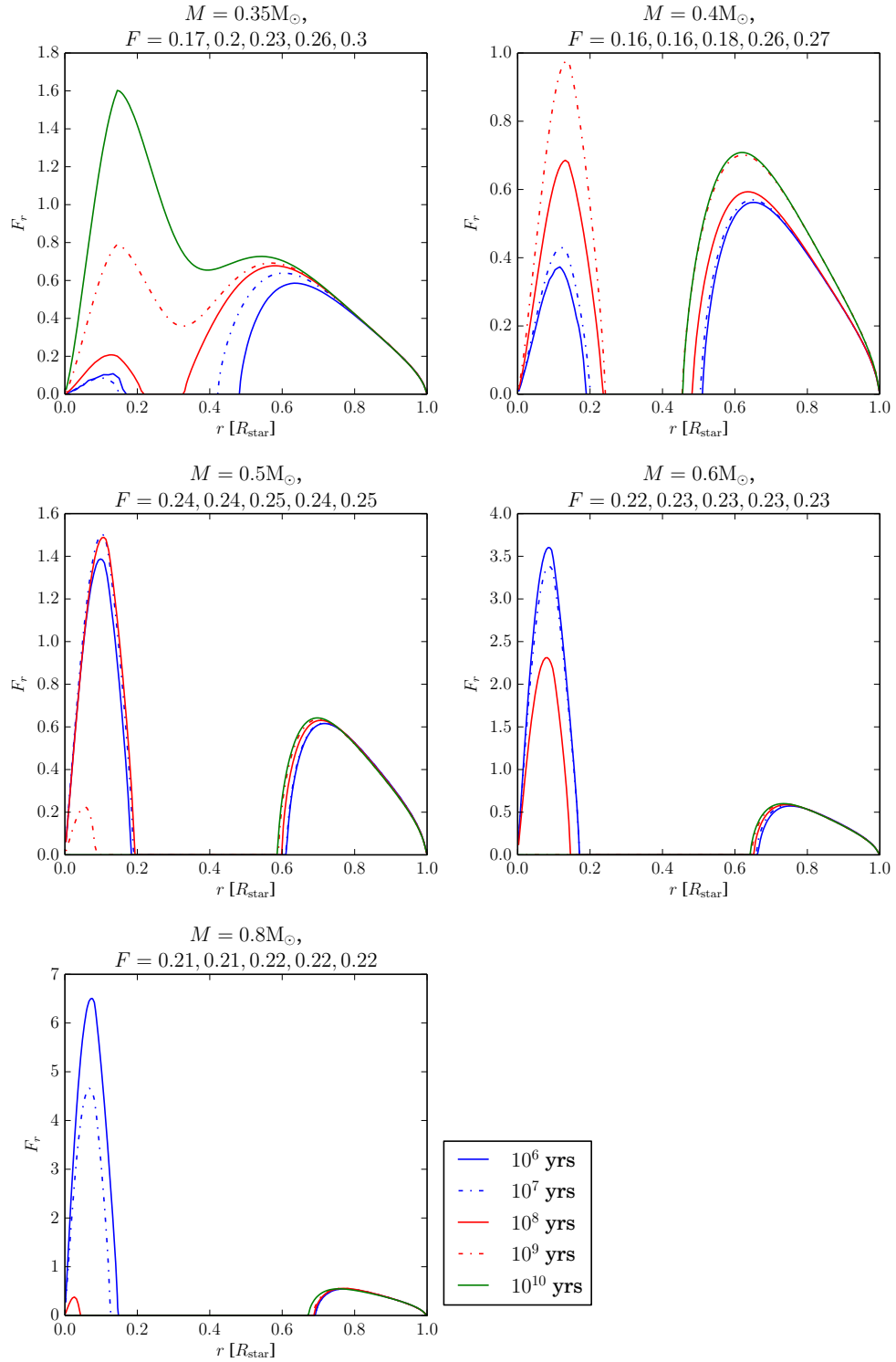


Figure 4.7b: **Spatial distribution of F_r for $0.35 M_{\odot} \leq M \leq 0.8 M_{\odot}$**
The value F_r is calculated according to equation 3.5. The values for F in the title are integrated values according to equation (3.6) for the ages 10^6 , 10^7 , 10^8 , 10^9 and 10^{10} years. The mixing-length parameter is $\alpha_{\text{MLT}} = 2.0$.

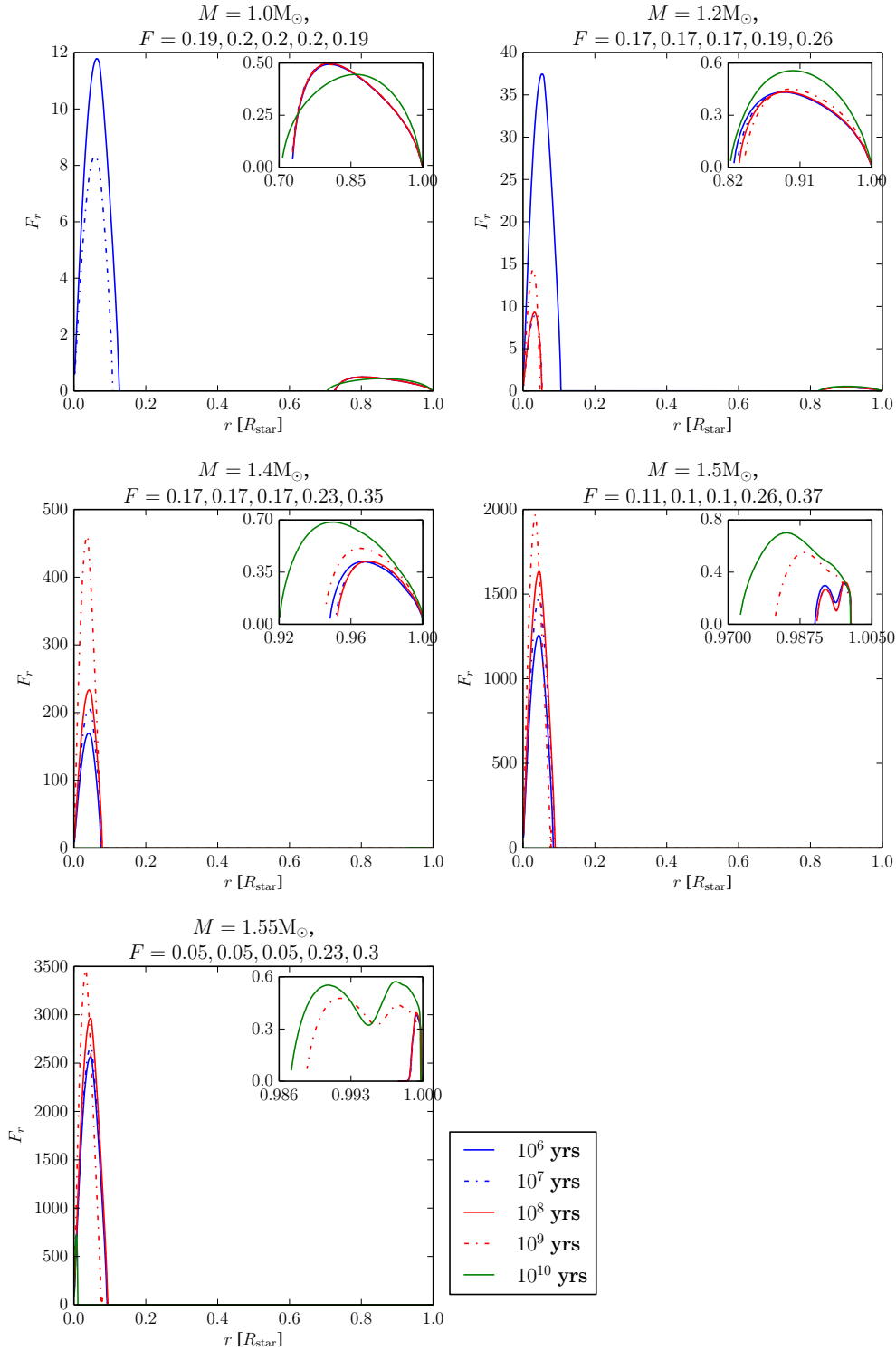


Figure 4.7c: **Spatial distribution of F_r for $1.0 M_{\odot} \leq M_{\odot} \leq 1.55 M_{\odot}$**
 The value F_r is calculated according to equation 3.5. The values for F in the title are integrated values according to equation (3.6) for the ages 10^6 , 10^7 , 10^8 , 10^9 and 10^{10} years. Shown in the inset is the convective envelope of the star. The mixing-length parameter is $\alpha_{\text{MLT}} = 2.0$.

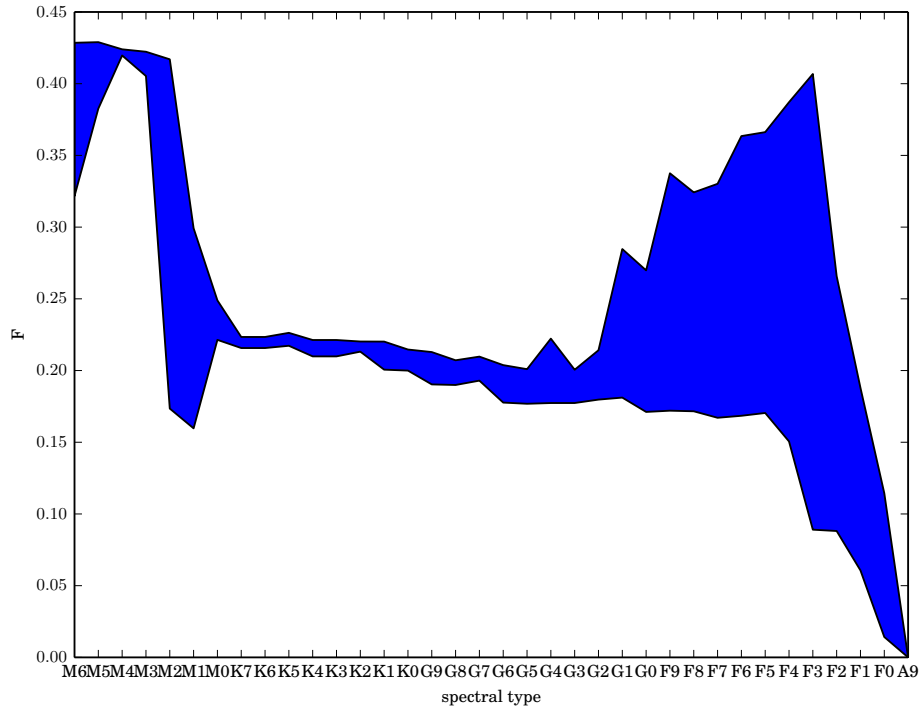


Figure 4.8: **Efficiency factors as a function of spectral type**

The values are taken from integration according to equations (3.5) and (3.6). y -ranges account for the fact that stars of different mass, age, and mixing-length parameter and therefore different F are assigned to the same spectral type. The assignment of model to spectral type is made via the effective temperature according to figure 4.2.

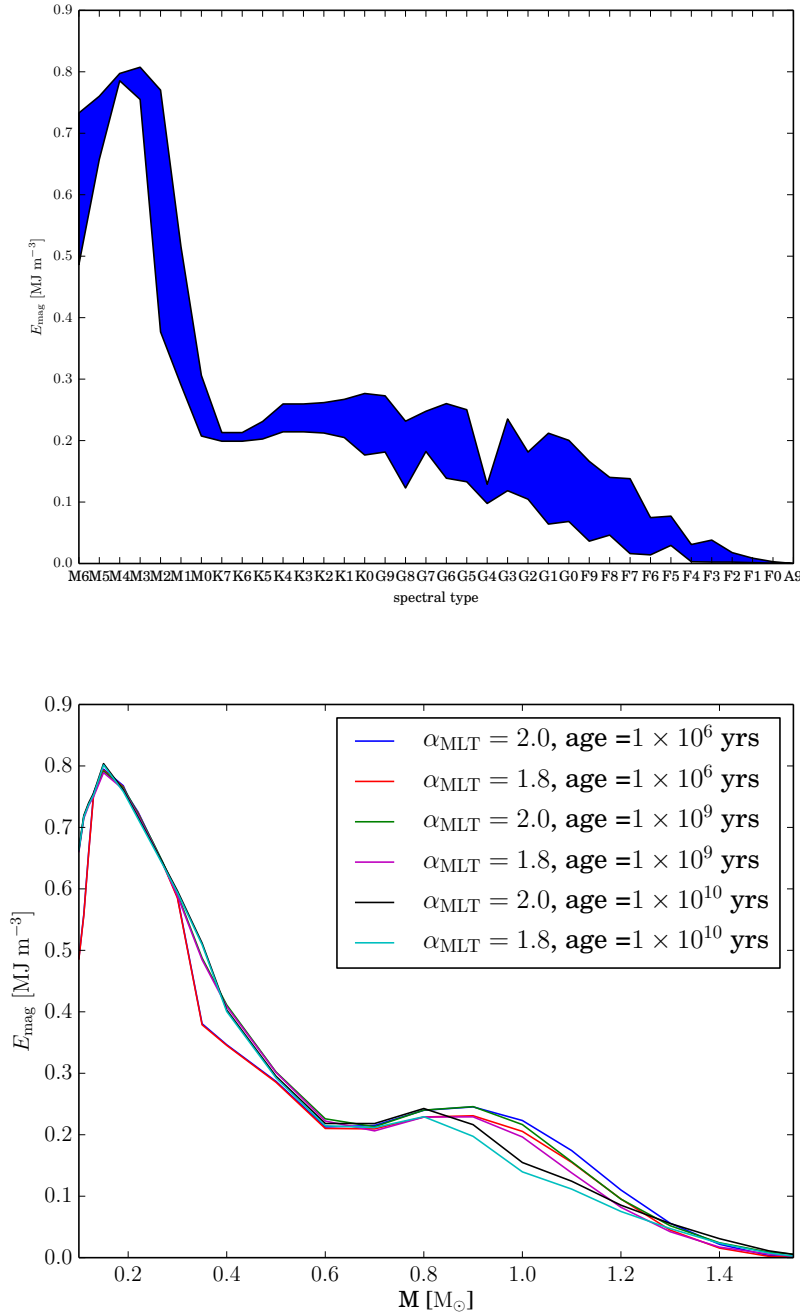


Figure 4.9: Magnetic energy density

In the upper plot it is shown as a function of spectral type, in the lower plot as a function of mass for three different ages and two mixing-length parameters. For f_{ohm} a value of one is assumed. The magnetic energy densities are calculated according to scaling law (2.26). y -ranges in the upper plot account for the fact that stars of different mass, age, and mixing-length parameter and therefore different E_{mag} are assigned to the same spectral type. The assignment of model to spectral type is made via the effective temperature according to figure 4.2.

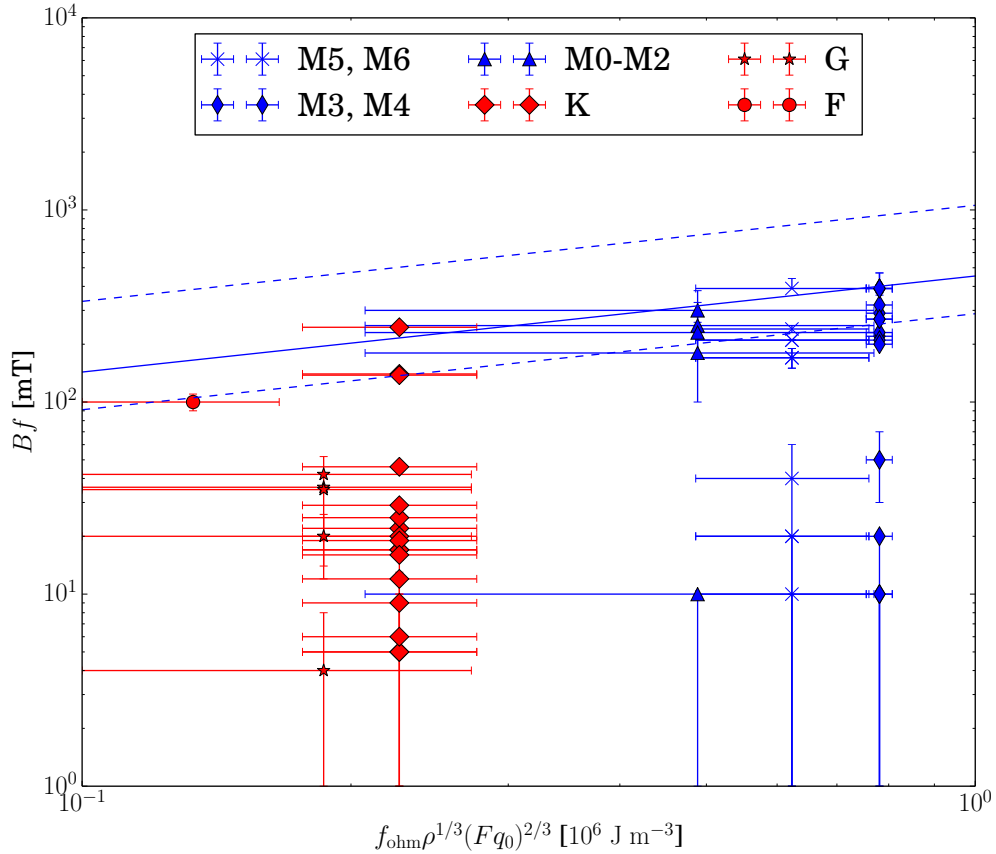


Figure 4.10: **Comparison with data from [23]**

The x -values are the computed values for magnetic energy density according to the scaling law (2.25). The x -errorbars are obtained by assigning models with different resulting magnetic energy densities to the same spectral type.

y -data and errors are from observations published in [1, 16, 20, 22, 24, 26, 28–30, 33] and collected in [23].

The blue solid line is the prediction $E_{\text{mag}} = \frac{(xB_s)^2}{2\mu_0}$, whereas the factor $x = 3.5$ is an assumption according to [8]. The dashed lines account for values of $x = 1.5$ (upper line) and $x = 5.5$ (lower line).

5 Discussion

5.1 Meaning of the results

The comparison in section 4.4.2 shows that the scaling law is valid as it predicts magnetic fields for stars which fit the observed fields within one order of magnitude. Hereby I confirm the results of [8] even though I found smaller values for the efficiency factor F . While they were found to lie in the range 0.69–1.22 I found a range of 0.1–0.43 whereupon I analysed stars in a wider mass range (0.1 – $1.55 M_{\odot}$ against 0.25 – $0.7 M_{\odot}$). A possible reason for this is that I used a different stellar evolution code which provides different profiles for the quantities like temperature and density. The scaling law predicts a maximum value for the magnetic energy density inside stars which can be produced by the dynamos of $0.81 \times 10^6 \text{ J/m}^3$ which corresponds to a field of 1.4 T. The maximum value for high mass stars ($M \geq 0.6 M_{\odot}$) is $0.28 \times 10^6 \text{ J/m}^3$ (corresponding field of 0.8 T). It is questionable what part of this magnetic field can actually be observed.

I extended the analysis towards larger stars with masses of more than $1.0 M_{\odot}$ where the convective envelope is comparatively small. The dynamo processes in these stars seem to be less effective at low ages but old stars in this mass range have similar F values as M stars despite the shallow convection zone (cf. figure 4.8). However, the scaling law predicts magnetic fields which are in the same order of magnitude as the fields of M stars and the field decreases with increasing mass (cf. figure 4.9).

The comparison with data also confirms the prediction that the scaling law is only applicable to fast rotators since slow rotators are not saturated. The reason that magnetic fields of some M stars in figure 4.10 are low compared to the scaling law (less than one kG) could be that these stars are old and therefore slow rotating in contrast to young, fast rotating M dwarfs which show magnetic fields of a few kG.

5.2 Open questions

For stars which are not fully convective I observed convective cores (cf. figures 4.7b and 4.7c) whose convective flux strength increases with mass. According to figure 2.1 convective cores are expected only in stars of spectral type A and earlier, here they occur in spectral type early-M which are about one order of magnitude less massive. Since the magnetic field which would be produced in these cores would be shielded by the radiative zone I neglect the cores in this study. However, it remains an open question if these cores are physically significant or a numerical issue.

An important question is which factor of the magnetic field is observable at the surface. In the plot 4.10 I adopted the assumption by [8] that the factor $x = B/B_s$ is 3.5 but it is unlikely that a fixed factor can be assumed.

6 Conclusion

I used a stellar evolution code, `MESA star`, to compute properties inside stars of different masses and ages. These calculations were used to compute magnetic fields according to a certain scaling law (2.25). In doing this I extended a former analysis of the same scaling law [8] towards higher masses.

My study confirms the results of the former analysis but also makes some predictions of the magnetic energy densities in higher mass stars which are lower by a factor of three to four compared with those of late type stars. The very thin convective envelopes in G and F stars still can produce magnetic fields in the kG-regime which are comparable to those of fully convective M stars.

Bibliography

- [1] Richard I. Anderson, Ansgar Reiners, and Sami K. Solanki. On detectability of Zeeman broadening in optical spectra of F- and G-dwarfs. *Astronomy & Astrophysics*, 522:A81, November 2010. ISSN 0004-6361, 1432-0746. doi: 10.1051/0004-6361/201014769. URL <http://arxiv.org/abs/1008.2213>. arXiv: 1008.2213.
- [2] Will T. Ball. Solar Basics | Imperial College London Astrophysics. URL <http://astro.ic.ac.uk/research/solar-basics>. Cited on June 28, 2016.
- [3] Kwing L. Chan and Sabatino Sofia. Validity Tests of the Mixing-Length Theory of Deep Convection. *Science*, 235(4787):465–467, January 1987. ISSN 0036-8075, 1095-9203. doi: 10.1126/science.235.4787.465. URL <http://science.sciencemag.org/content/235/4787/465>.
- [4] Paul Charbonneau. *Solar and Stellar Dynamos: Saas-Fee Advanced Course 39 Swiss Society for Astrophysics and Astronomy*. Number 39 in Saas-Fee Advanced Courses. Springer, Berlin, 2013. ISBN 978-3-642-32093-4.
- [5] Ulrich R. Christensen. Dynamo Scaling Laws and Applications to the Planets. *Space Science Reviews*, 152(1-4):565–590, July 2009. ISSN 0038-6308, 1572-9672. doi: 10.1007/s11214-009-9553-2. URL <http://link.springer.com/article/10.1007/s11214-009-9553-2>.
- [6] Ulrich R. Christensen and Julien Aubert. Scaling properties of convection-driven dynamos in rotating spherical shells and application to planetary magnetic fields. *Geophysical Journal International*, 166(1):97–114, July 2006. ISSN 0956540X, 1365246X. doi: 10.1111/j.1365-246X.2006.03009.x. URL <http://gji.oxfordjournals.org/cgi/doi/10.1111/j.1365-246X.2006.03009.x>.
- [7] Ulrich R. Christensen and Andreas Tilgner. Power requirement of the geodynamo from ohmic losses in numerical and laboratory dynamos. *Nature*, 429

Bibliography

- (6988):169–171, May 2004. ISSN 0028-0836. doi: 10.1038/nature02508. URL <http://dx.doi.org/10.1038/nature02508>.
- [8] Ulrich R. Christensen, Volkmar Holzwarth, and Ansgar Reiners. Energy flux determines magnetic field strength of planets and stars. *Nature*, 457(7226): 167–169, January 2009. ISSN 0028-0836. doi: 10.1038/nature07626. URL <http://www.nature.com/naturecom.han.sub.uni-goettingen.de/nature/journal/v457/n7226/full/nature07626.html>.
- [9] J. F. Donati and J. D. Landstreet. Magnetic fields of non-degenerate stars. *Annual Review of Astronomy and Astrophysics*, 47(1):333–370, September 2009. ISSN 0066-4146, 1545-4282. doi: 10.1146/annurev-astro-082708-101833. URL <http://arxiv.org/abs/0904.1938>. arXiv: 0904.1938.
- [10] F. R. Ferraro, E. Valenti, O. Straniero, and L. Origlia. An empirical calibration of the mixing-length parameter alpha. *The Astrophysical Journal*, 642(1):225–229, May 2006. ISSN 0004-637X, 1538-4357. doi: 10.1086/500803. URL <http://arxiv.org/abs/astro-ph/0601159>. arXiv: astro-ph/0601159.
- [11] David Gubbins. Geodynamo, Dimensional Analysis And Timescales. In David Gubbins and Emilio Herrero-Bervera, editors, *Encyclopedia of Geomagnetism and Paleomagnetism*, pages 297–300. Springer Netherlands, 2007. ISBN 978-1-4020-3992-8 978-1-4020-4423-6. URL http://link.springer.com/referenceworkentry/10.1007/978-1-4020-4423-6_109. DOI: 10.1007/978-1-4020-4423-6_109.
- [12] Chris Jones. Geodynamo. In David Gubbins and Emilio Herrero-Bervera, editors, *Encyclopedia of Geomagnetism and Paleomagnetism*, pages 287–296. Springer Netherlands, 2007. ISBN 978-1-4020-3992-8 978-1-4020-4423-6. URL http://link.springer.com/referenceworkentry/10.1007/978-1-4020-4423-6_108. DOI: 10.1007/978-1-4020-4423-6_108.
- [13] Scott J. Kenyon and Lee Hartmann. Pre-Main-Sequence Evolution in the Taurus-Auriga Molecular Cloud. *The Astrophysical Journal Supplement Series*, 101:117, November 1995. ISSN 0067-0049. doi: 10.1086/192235. URL <http://adsabs.harvard.edu/abs/1995ApJS..101..117K>.

- [14] Rudolf Kippenhahn. *Stellar Structure and Evolution*. Astronomy and Astrophysics Library. Springer, Berlin, 2nd ed. 2013. edition, 2013. ISBN 978-3-642-30304-3.
- [15] Maria A. Loukitcheva, Sami K. Solanki, and Stephen M. White. The relationship between chromospheric emissions and magnetic field strength. *Astronomy and Astrophysics*, 497(1):273–285, April 2009. ISSN 0004-6361, 1432-0746. doi: 10.1051/0004-6361/200811133. URL <http://arxiv.org/abs/0910.1985>. arXiv: 0910.1985.
- [16] Geoffrey W. Marcy and Gibor Basri. Physical realism in the analysis of stellar magnetic fields. II - K dwarfs. *The Astrophysical Journal*, 345:480–488, October 1989. ISSN 0004-637X. doi: 10.1086/167921. URL <http://adsabs.harvard.edu/abs/1989ApJ...345..480M>.
- [17] Bill Paxton, Lars Bildsten, Aaron Dotter, Falk Herwig, Pierre Lesaffre, and Frank Timmes. Modules for Experiments in Stellar Astrophysics (MESA). *The Astrophysical Journal Supplement Series*, 192:3, January 2011. ISSN 0067-0049. doi: 10.1088/0067-0049/192/1/3. URL <http://adsabs.harvard.edu/abs/2011ApJS...192....3P>.
- [18] Bill Paxton, Matteo Cantiello, Phil Arras, Lars Bildsten, Edward F. Brown, Aaron Dotter, Christopher Mankovich, M. H. Montgomery, Dennis Stello, F. X. Timmes, and Richard Townsend. Modules for Experiments in Stellar Astrophysics (MESA): Planets, Oscillations, Rotation, and Massive Stars. *The Astrophysical Journal Supplement Series*, 208:4, September 2013. ISSN 0067-0049. doi: 10.1088/0067-0049/208/1/4. URL <http://adsabs.harvard.edu/abs/2013ApJS...208....4P>.
- [19] Bill Paxton, Pablo Marchant, Josiah Schwab, Evan B. Bauer, Lars Bildsten, Matteo Cantiello, Luc Dessart, R. Farmer, H. Hu, N. Langer, R. H. D. Townsend, Dean M. Townsley, and F. X. Timmes. Modules for Experiments in Stellar Astrophysics (MESA): Binaries, Pulsations, and Explosions. *The Astrophysical Journal Supplement Series*, 220:15, September 2015. ISSN 0067-0049. doi: 10.1088/0067-0049/220/1/15. URL <http://adsabs.harvard.edu/abs/2015ApJS...220...15P>.
- [20] N. Phan-Bao, J. Lim, J.-F. Donati, C. M. Johns-Krull, and E. L. Martin.

- Magnetic Field Topology in Low-Mass Stars: Spectropolarimetric Observations of M Dwarfs. *The Astrophysical Journal*, 704(2):1721–1729, October 2009. ISSN 0004-637X, 1538-4357. doi: 10.1088/0004-637X/704/2/1721. URL <http://arxiv.org/abs/0909.2355>. arXiv: 0909.2355.
- [21] N. Pizzolato, A. Maggio, G. Micela, S. Sciortino, and P. Ventura. The stellar activity-rotation relationship revisited: Dependence of saturated and non-saturated X-ray emission regimes on stellar mass for late-type dwarfs. *Astronomy and Astrophysics*, 397:147–157, January 2003. ISSN 0004-6361. doi: 10.1051/0004-6361:20021560. URL <http://adsabs.harvard.edu/abs/2003A%26A...397..147P>.
- [22] A. Reiners and G. Basri. The First Direct Measurements of Magnetic Fields on Very Low-Mass Stars. *The Astrophysical Journal*, 656(2):1121–1135, February 2007. ISSN 0004-637X, 1538-4357. doi: 10.1086/510304. URL <http://arxiv.org/abs/astro-ph/0610365>. arXiv: astro-ph/0610365.
- [23] Ansgar Reiners. Observations of Cool-Star Magnetic Fields. *Living Reviews in Solar Physics*, 9, 2012. ISSN 1614-4961. doi: 10.12942/lrsp-2012-1. URL <http://www.livingreviews.org/lrsp-2012-1>. Cited on Marc 27, 2016.
- [24] Ansgar Reiners and Gibor Basri. On the magnetic topology of partially and fully convective stars. *Astronomy and Astrophysics*, 496(3):787–790, March 2009. ISSN 0004-6361, 1432-0746. doi: 10.1051/0004-6361:200811450. URL <http://arxiv.org/abs/0901.1659>. arXiv: 0901.1659.
- [25] Ansgar Reiners, Gibor Basri, and Matthew K. Browning. Evidence for Magnetic Flux Saturation in Rapidly Rotating M Stars. *The Astrophysical Journal*, 692(1):538–545, February 2009. ISSN 0004-637X, 1538-4357. doi: 10.1088/0004-637X/692/1/538. URL <http://arxiv.org/abs/0810.5139>. arXiv: 0810.5139.
- [26] I. Rueddi, S. K. Solanki, G. Mathys, and S. H. Saar. Magnetic field measurements on moderately active cool dwarfs. *Astronomy and Astrophysics*, 318:429–442, February 1997. ISSN 0004-6361. URL <http://adsabs.harvard.edu/abs/1997A%26A...318..429R>.
- [27] C. T. Russell. Re-evaluating Bode’s law of planetary magnetism. *Nature*, 272(5649):147–148, March 1978. doi: 10.1038/272147a0. URL

- <http://www.nature.com/naturecom.han.sub.uni-goettingen.de/nature/journal/v272/n5649/abs/272147a0.html>.
- [28] S. H. Saar. New Infrared Measurements of Magnetic Fields on Cool Stars. *Infrared Solar Physics*, 154:493, 1994. URL <http://adsabs.harvard.edu/abs/1994IAUS...154..493S>.
- [29] S. H. Saar and S. L. Baliunas. The Magnetic Cycle of Kappa Ceti. *The Solar Cycle*, 27:197–202, 1992. URL <http://adsabs.harvard.edu/abs/1992ASPC...27..197S>.
- [30] S.H. Saar. Recent measurements of stellar magnetic fields. In Yutaka Uchida, Takeo Kosugi, and Hugh S. Hudson, editors, *Magnetodynamic Phenomena in the Solar Atmosphere: Prototypes of Stellar Magnetic Activity*, pages 367–374. Springer Science & Business Media, September 1996. ISBN 978-0-7923-4176-5.
- [31] S. V. Starchenko and C. A. Jones. Typical Velocities and Magnetic Field Strengths in Planetary Interiors. *Icarus*, 157(2):426–435, June 2002. ISSN 0019-1035. doi: 10.1006/icar.2002.6842. URL <http://www.sciencedirect.com/science/article/pii/S0019103502968429>.
- [32] David J. Stevenson. Turbulent thermal convection in the presence of rotation and a magnetic field: A heuristic theory. *Geophysical & Astrophysical Fluid Dynamics*, 12(1):139–169, January 1979. ISSN 0309-1929. doi: 10.1080/03091927908242681. URL <http://dx.doi.org/10.1080/03091927908242681>.
- [33] Jeff A. Valenti, Geoffrey W. Marcy, and Gibor Basri. Infrared Zeeman analysis of epsilon Eridani. *The Astrophysical Journal*, 439:939–956, February 1995. ISSN 0004-637X. doi: 10.1086/175231. URL <http://adsabs.harvard.edu/abs/1995ApJ...439..939V>.
- [34] Eric W. Weisstein. Density Scale Height - from eric weisstein's world of physics. <http://scienceworld.wolfram.com/physics/DensityScaleHeight.html>. cited on April 5, 2016.
- [35] Keke Zhang. Core Convection. In David Gubbins and Emilio Herrero-Bervera, editors, *Encyclopedia of Geomagnetism and Paleomagnetism*, pages 80–82. Springer Netherlands, 2007. ISBN 978-1-4020-3992-8 978-1-4020-4423-6. URL http://link.springer.com/referenceworkentry/10.1007/978-1-4020-4423-6_34. DOI: 10.1007/978-1-4020-4423-6_34.

Acknowledgement

I wish to thank Dr. Denis Shulyak who supported me at any time, Prof. Dr. Ansgar Reiners who gave me the opportunity to work in his group and Prof. Dr. Ulrich Christensen who patiently answered to all my questions according his papers.

Special thanks are dedicated to my proofreader, namely Freya Anders, and my parents for always supporting me.

Erklärung nach §13(9) der Prüfungs- und Studienordnung für den Bachelor-Studiengang „Physik“ sowie den konsekutiven Master-Studiengang „Physik“ der Georg-August-Universität Göttingen:

Hiermit erkläre ich, dass ich diese Abschlussarbeit selbständig verfasst habe, keine anderen als die angegebenen Quellen und Hilfsmittel benutzt habe und alle Stellen, die wörtlich oder sinngemäß aus veröffentlichten Schriften entnommen wurden, als solche kenntlich gemacht habe.

Darüberhinaus erkläre ich, dass diese Abschlussarbeit nicht, auch nicht auszugsweise, im Rahmen einer nichtbestanden Prüfung an dieser oder einer anderen Hochschule eingereicht wurde.

Göttingen, den 19. Juli 2016

(Merten Nikolay Dahlkemper)